



Dual-distribution discrepancy with self-supervised refinement for anomaly detection in medical images

Yu Cai^a, Hao Chen^{b,*}, Xin Yang^c, Yu Zhou^c, Kwang-Ting Cheng^{a,b}

^aDepartment of Electronic and Computer Engineering, The Hong Kong University of Science and Technology, Hong Kong, China

^bDepartment of Computer Science and Engineering, The Hong Kong University of Science and Technology, Hong Kong, China

^cSchool of Electronic Information and Communications, Huazhong University of Science and Technology, Wuhan 430074, China

ARTICLE INFO

Article history:

Received 1 May 2013

Received in final form 10 May 2013

Accepted 13 May 2013

Available online 15 May 2013

Communicated by S. Sarkar

Keywords:

Anomaly detection

Reconstruction networks

Self-supervised learning

Benchmark

ABSTRACT

Medical anomaly detection is a crucial yet challenging task aiming at recognizing abnormal images to assist diagnosis. Due to the high-cost annotations of abnormal images, most methods utilize only known normal images during training and identify samples not conforming to the normal profile as anomalies in the testing phase. A large number of readily available unlabeled images containing anomalies are thus ignored in the training phase, restricting their performance. To solve this problem, we propose the Dual-distribution Discrepancy for Anomaly Detection (DDAD), utilizing both known normal images and unlabeled images. Two modules are designed to model the normative distribution of normal images and the unknown distribution of both normal and unlabeled images, respectively, using ensembles of reconstruction networks. Subsequently, intra-discrepancy of the normative distribution module, and inter-discrepancy between the two modules are designed as anomaly scores. Furthermore, an Anomaly Score Refinement Net (ASR-Net) trained via self-supervised learning is proposed to refine the two anomaly scores. For evaluation, five medical datasets including chest X-rays, brain MRIs and retinal fundus images are organized as benchmarks. Experiments on these benchmarks demonstrate our method achieves significant gains and outperforms state-of-the-art methods. Code and organized benchmarks will be available at <https://github.com/caiyu6666/DDAD-ASR>.

© 2022 Elsevier B. V. All rights reserved.

1. Introduction

Thanks to the cost-effectiveness and a reasonable sensitivity to a wide variety of pathologies, medical imaging is of vital importance to the diagnosis of various diseases. Take the case of chest X-rays (CXRs), which is the most commonly performed radiological exam (Çallı et al., 2021) and has been widely applied for the detection of tens of lung diseases such as pneumonia, nodule, lung opacity, pneumothorax, etc. To alleviate

radiologists' reading burden and improve diagnosis efficiency, automatic CXR analysis using deep learning is becoming popular (Luo et al., 2020, 2021). However, the annotations of medical images is difficult, relies on the experience of professional experts, and is time-consuming and labor-intensive, which motivates the development of an intelligent system helping radiologists detect and localize potential abnormalities in medical images automatically using few or even no annotations.

As the annotations of normal images from healthy subjects are relatively easy to obtain while anomalies are complex, various and usually difficult to collect, most existing methods consider anomaly detection as a one-class classification (OCC) problem (Ruff et al., 2018), where only normal images are uti-

*Corresponding author.
e-mail: jhc@cse.ust.hk (Hao Chen)

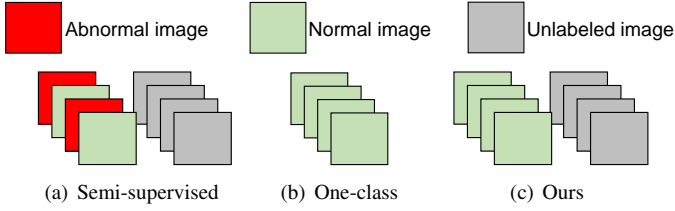


Fig. 1. Different training modes for medical anomaly detection. (a) Semi-supervised mode can make use of unlabeled images, but labeled abnormal images are necessary, thus infeasible. (b) One-Class Classification mode utilizes only normal images, which is the most popular but wasting unlabeled images. (c) Our proposed mode utilizes both normal images and unlabeled images.

lized for training and samples not conforming to normal profile are identified as anomalies in the testing phase, thus no need for annotations of abnormal images during training. This type of setting has been extensively studied in anomaly detection for both computer vision tasks (Ruff et al., 2021) and medical image analysis (Baur et al., 2021). Nevertheless, due to the lack of training on real abnormal images, the discriminative capability of these methods is limited. Meanwhile, an important fact is ignored that different from the application scenarios in computer vision tasks like industrial defect detection (Bergmann et al., 2019) and video anomaly detection (Sultani et al., 2018; Li et al., 2013) where abnormal cases are rare, there are plenty of readily available unlabeled images with a certain anomaly rate (AR) in medical clinical practice. These unlabeled images containing rich anomalous features are wasted by methods based on the OCC setting, which restricts the performance of anomaly detection. Unfortunately, up to now, there is no notable work leveraging these unlabeled images for anomaly detection effectively.

Based on this observation, we raise a problem: whether unlabeled images can provide effective information of abnormalities as a complement of normal images to improve the performance of anomaly detection? Motivated by this, in this work, we propose the Dual-distribution Discrepancy for Anomaly Detection (DDAD), where a novel training mode that takes advantage of both known normal images and unlabeled images is explored. The proposed training mode is more reasonable and consistent with the medical clinical practice, whose comparison with existing modes is shown in Fig. 1. Recently, semi-supervised methods (Fig. 1(a)) have been widely used for medical images analysis (Cheplygina et al., 2019). Although they can make use of unlabeled images, the labeled abnormal images are necessary, which is high-cost and infeasible for anomaly detection. The OCC mode (Fig. 1(b)) is feasible and has been extensively studied in most existing anomaly detection works, but plenty of unlabeled images are ignored. Our proposed mode (Fig. 1(c)) combines the advantages of both, utilizing unlabeled images without the need for labeled abnormal images.

Fig. 2 illustrates the overview of our DDAD. To capture information from both known normal images and unlabeled images, we design two modules, normative distribution module (NDM) and unknown distribution module (UDM), each of which is an ensemble of several reconstruction networks

with the same architecture. During training, NDM models the distribution of only known normal images, while UDM takes both known normal and unlabeled images as inputs, capturing anomalous features from unlabeled images in some way. Based on the theory of *Deep Ensemble* (Lakshminarayanan et al., 2017), as NDM is trained on only normal images, the reconstructions' variance will be high in unseen abnormal regions, thus the *intra-discrepancy* inside NDM is used as an anomaly score (AS). Besides, as UDM captures some anomalous features from unlabeled images that NDM never sees, high discrepancy between their outputs will also derive in these abnormal regions. Therefore, the *inter-discrepancy* between the two modules is applied as another AS. To further refine and fuse the aforementioned two anomaly scores, we design an Anomaly Score Refinement Net (ASR-Net), which is trained via self-supervised learning. Compared with other self-supervised anomaly detection methods, our ASR-Net learns to map the original AS to the final accurate abnormal regions, rather than detect the synthetic abnormal patterns, leading to better performance. Considering the lack of public available benchmarks for medical anomaly detection, we for the first time collect and organize five medical datasets including CXRs, brain MRIs and retinal fundus images for evaluation and release them to facilitate other researchers to evaluate their methods fairly. Experiments on these five datasets demonstrate the effectiveness of the proposed DDAD, which outperforms existing state-of-the-art methods even if without unlabeled images, while unlabeled images can be utilized to further improve our performance by a large margin.

Our main contributions are summarized as follows:

- We propose to use the ensembles of reconstruction networks to model the distribution of training data in an unsupervised fashion. Based on it, the normative distribution module (NDM) and unknown distribution module (UDM) are designed to model the distribution of only known normal images and the distribution of both known normal images and unlabeled images, respectively. It is the first time that unlabeled images are utilized to improve the performance of anomaly detection.
- Two novel and powerful anomaly scores, the *intra-discrepancy* inside NDM and *inter-discrepancy* between the two modules, are proposed to indicate anomalies.
- An Anomaly Score Refinement Net (ASR-Net) trained via self-supervised learning is proposed to refine and fuse the aforementioned two anomaly scores. Different from existing self-supervised anomaly detection methods that learn to detect the synthetic abnormal patterns, it learns to map the original AS to the final accurate abnormal regions, achieving better performance.
- Five medical datasets including three modalities are collected and organized by us and released as benchmarks for medical anomaly detection, which will facilitate the fair comparison of other methods as there are few related benchmarks previously.

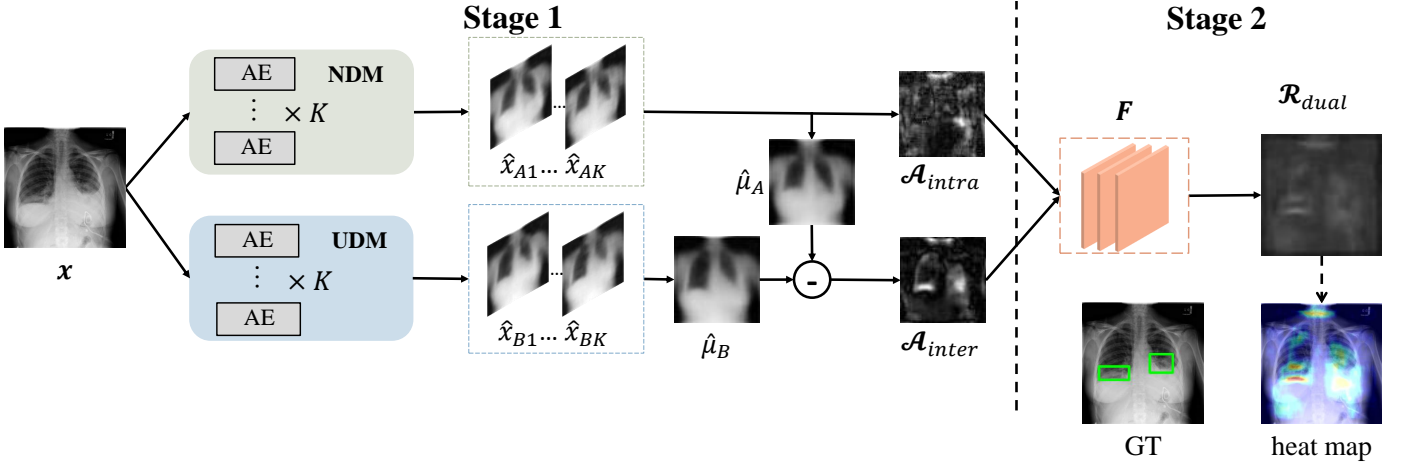


Fig. 2. Overview of the proposed DDAD. In the Stage 1, NDM and UDM model the distribution of known normal images and the distribution of known normal and unlabeled images, respectively. Then the intra-discrepancy inside NDM and inter-discrepancy between the two modules are designed as anomaly scores. In the Stage 2, the two anomaly scores are refined and fused by the ASR-Net $F(\cdot)$, deriving the final prediction \mathcal{R}_{dual} .

- Extensive experiments on the five medical datasets demonstrate the proposed method achieves consistent, significant gains and outperforms state-of-the-art methods in anomaly detection.

A preliminary version of this work was early accepted in MICCAI 2022 (Cai et al., 2022). In this paper, the major extensions include designing a new module, i.e., ASR-Net, that improves the performance and robustness significantly, adding much more experiments on more datasets containing different modalities, elaborating analysis and providing a more comprehensive literature review.

The rest of this paper is organized as follows: Section 2 describes related works. Section 3 describes the proposed DDAD methods with our ASR-Net in details. In Section 4, extensive experiments on five datasets are conducted to demonstrate the effectiveness of our proposed method. We conclude our work in Section 6.

2. Related work

Anomaly detection aims at finding patterns in data that do not conform to expected behavior (Chandola et al., 2009). It is a promising field that has been widely applied in a variety of domains. Due to the difficulty of collecting abundant annotated various abnormal samples, almost all the existing works utilize only normal images during training, which is the well-known OCC setting (Ruff et al., 2018).

Intuitively, anomalies that deviated from the distribution of normal samples can be separated from normal samples by a discriminative hyperplane, based on which the classical method, one-class support vector machine (OC-SVM) (Schölkopf et al., 1999), was proposed. Its derived deep one-class SVDD (Ruff et al., 2018) utilizes convolutional neural networks (CNNs) to constrain the normal samples in a hypersphere with minimum volume, handling high-dimensional data better but suffering from the problem of mode collapse. Recently, most state-of-the-art methods for anomaly detection focus on reconstruction

and self-supervised learning, which are also what this paper mainly discusses.

2.1. Reconstruction-based Anomaly Detection

Reconstruction-based methods are one of the most popular family in anomaly detection, especially for medical images (Baur et al., 2021). They usually utilize generative models, such as generative adversarial networks (GANs) (Goodfellow et al., 2014), auto-encoders (AEs) or their variants, to learn a mapping function to reconstruct normal images, while the unseen abnormal images are assumed unable to be reconstructed well by these models trained with only normal images, and in turn yield high reconstruction error.

Specifically, Schlegl et al. (2017) firstly used GANs for anomaly detection. They proposed AnoGAN to learn the manifold of normal images. For a query image, a latent feature is found via iterative process to generate an image most similar to the query image. The query image will be identified as abnormal if there is a high difference with the best generated image. To replace the time-consuming iterative process in the testing phase, Schlegl et al. (2019) further utilized an encoder to learn the mapping from retinal OCT image to latent space, and derived the fast version of AnoGAN, termed f-AnoGAN. However, these GAN-based methods could suffer from memorization pitfalls, causing that reconstructions often differ anatomically from the actual input.

Various approaches also used variants of AEs for anomaly detection, including the Variational AE (VAE) (Zimmerer et al., 2018), Adversarial AE (AAE) (Chen and Konukoglu, 2018), Vector Quantized VAE (VQ-VAE) (Marimont and Tarroni, 2021), etc. To avoid abnormal images being well reconstructed, Gong et al. (2019) proposed to augment the AE with a memory module, which can store the latent features of normal training samples. The reconstruction is obtained from a few most relevant memory records, thus tend to be close to a normal image and enlarge the reconstruction errors of abnormal images. Compared with GAN-based methods, AE-based methods could preserve more anatomical coherence, but usually generate

blurry reconstructions (Baur et al., 2021), leading to false positive detection around high-frequency regions (e.g., boundary). To mitigate this problem, Mao et al. (2020) proposed to automatically estimate the pixel-level uncertainty of reconstruction using AE, which is used to normalize the reconstruction error and suppress the false positive detection in CXR significantly.

Recently, incorporating adversarial training into AEs is popular, which combines the advantages of both. Baur et al. (2018) demonstrated that AEs with spatial bottlenecks can reconstruct important fine details better than those with dense bottlenecks, and combined the spatial VAE with GAN to improve realism of the reconstructed normal samples for anomaly detection in brain MRI. In addition to the adversarial training, Akcay et al. (2018) used an extra encoder to map the reconstructed image to latent space again, and minimized reconstruction errors in both image space and latent space during training to aid in learning the data distribution for the normal samples. Zaheer et al. (2020) proposed to transform the fundamental role of a discriminator from identifying real and fake data to distinguishing between good and bad quality reconstructions, which is highly desirable in anomaly detection as a trained AE would not produce as good reconstruction for abnormal data as it would for the normal data conforming to the learned representations.

2.2. Self-Supervised Learning-based Anomaly Detection

Self-supervised learning (Jing and Tian, 2020) refers to learning methods in which networks are explicitly trained using pretext tasks with generated pseudo labels, which is also extensively studied in anomaly detection. Sohn et al. (2020) proposed to first learn self-supervised representations from one-class data, and then build one-class classifiers on learned representations. Based on the proposed framework, they applied *distribution augmentation* (Jun et al., 2020) for one-class contrastive learning to reduce the uniformity of representations. Further, Tian et al. (2021) combined the distribution-augmented contrastive learning (Sohn et al., 2020), augmentation prediction (Golan and El-Yaniv, 2018), and position prediction (Dorersch et al., 2015) to learn feature representations for anomaly-sensitive detection models. Except for aforementioned contrastive learning methods, some works (Li et al., 2021; Tan et al., 2020, 2021) try to synthesize defects manually for training models to detect irregularities. Various image processing approaches were designed to synthesize abnormal images, including CutPaste (Li et al., 2021), Foreign Patch Interpolation (Tan et al., 2020), Poisson Image Interpolation (Tan et al., 2021), etc. However, these methods may not generalize well due to the reliance on the similarity between synthetic abnormal patterns and the real anomalies.

2.3. Ensemble-based Uncertainty Estimates

Deep Ensemble (Lakshminarayanan et al., 2017) is a simple but effective method for uncertainty estimates of deep neural networks, where high uncertainty will be expressed on out-of-distribution (OOD) samples. It has been successfully applied in the fields of open-set recognition and active learning (Beluch et al., 2018). However, the supervised training like semantic segmentation or classification is required in these methods, which is always not desirable in anomaly detection.

Recently, Bergmann et al. (2020) proposed to utilize feature vectors of pretrained networks on normal regions as surrogate labels for the training of an ensemble of student networks, whose predictive variance was used as an AS to segment anomalous regions. It successfully designed the ensemble-based method for industrial anomaly detection with no demand for labels, but required a powerful pretrained model, such as networks trained on ImageNet (Krizhevsky et al., 2012).

2.4. Summary

In summary, almost all previous works only used normal images for training, while plenty of unlabeled images in clinical practice were ignored. To take advantage of these unlabeled images, we design the NDM and UDM, both of which are ensembles of several reconstruction networks, to model the distribution of available training images. Specifically, NDM models the distribution of known normal images, while the UDM models the distribution of both known normal images and unlabeled images. Then the *intra-discrepancy* inside NDM and *inter-discrepancy* between the two modules are used as AS.

Compared with previous reconstruction-based methods (Baur et al., 2021), our scores are the discrepancy among outputs of network ensembles, rather than discrepancy between the input and output. Therefore, more information can be captured, while the high reconstruction errors in normal regions, caused by reconstruction ambiguity or memorization pitfalls, can be mitigated in some way. Compared with existing ensemble-based methods (Bergmann et al., 2020), we innovatively use reconstruction networks as the basic models for ensemble, which can be trained in an unsupervised fashion based on images themselves, i.e., reconstruction. Therefore, neither labels nor pretrained models are required, making our method can be applied in various scenarios more easily, including but not limited to medical anomaly detection.

Moreover, the ASR-Net trained via self-supervised learning is proposed to refine and fuse the designed two anomaly scores. Different from existing self-supervised anomaly detection methods that require realistic pseudo abnormal images, it learns to map the original AS to the final accurate abnormal regions, thus insensitive to the synthetic abnormal images and yielding better generalization.

3. Method

3.1. Problem Definition

In this section, we will first give the definition of the anomaly detection problem. Difference between our setting and previous setting will also be clarified.

Previously, most existing works formulate the anomaly detection as an OCC problem. That is, given a normal dataset $D_n = \{\mathbf{x}_{ni}\}_{i=1}^N$ with N normal images, and a test dataset $D_t = \{(\mathbf{x}_{ti}, y_i)\}_{i=1}^T$ with T annotated normal or abnormal images, where $y_i \in \{0, 1\}$ is the image label (0 for normal image and 1 for abnormal image), the goal is to train a model based on the normal image set D_n which can identify anomalies in the test dataset D_t during inference.

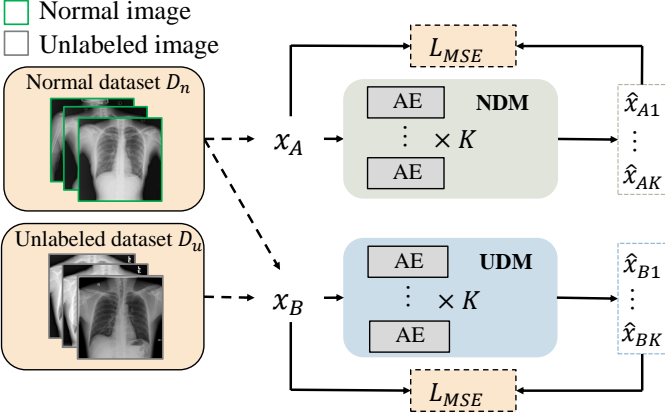


Fig. 3. Illustration of training NDM and UDM.

Different from previous works, our proposed DDAD method makes full use of the unlabeled images in clinical practice. Specifically, except for the normal dataset D_n , we also utilize a readily available unlabeled dataset $D_u = \{x_{ui}\}_{i=1}^M$ with M unlabeled images including both normal and abnormal images, to improve the performance of anomaly detection.

3.2. Dual-distribution Modeling

As shown in Fig. 2, we use two modules, NDM and UDM, in the Stage 1 to model the dual-distribution, whose training process is illustrated in Fig. 3. Each module is an ensemble of K reconstruction networks with the same architecture but different random initialization of parameters and random shuffling of training samples, trained by the Mean Squared Error (MSE) Loss to minimize reconstruction errors on the training set. Specifically, NDM is trained on only normal dataset D_n as:

$$\mathcal{L}_{NDM} = \frac{1}{N} \sum_{x_A \in D_n} \sum_{i=1}^K \|x_A - \hat{x}_{Ai}\|^2, \quad (1)$$

where N is the size of the normal dataset D_n , x_A is the input training image of NDM, and \hat{x}_{Ai} is the reconstruction of x_A from the i -th network in NDM. Similarly, the loss function of UDM trained on both normal image dataset D_n and unlabeled dataset D_u can be written as:

$$\mathcal{L}_{UDM} = \frac{1}{N+M} \sum_{x_B \in D_n \cup D_u} \sum_{i=1}^K \|x_B - \hat{x}_{Bi}\|^2. \quad (2)$$

Through this way, NDM models the distribution of known normal images while UDM captures effective information of abnormalities from the unlabeled dataset as a complement of normal images.

3.3. Dual-distribution Discrepancy-based Anomaly Scores

Given a testing image x , the pixel-wise reconstruction error $\mathcal{A}_{rec}^p = (x^p - \hat{x}^p)^2$ has been widely used as the AS. In this work, we design two innovative and effective anomaly scores based on the proposed ensemble modules.

Previously, ensemble-based methods train the ensemble networks via supervised tasks like classification or regression, then

utilize their output variance to identify OOD samples (Lakshminarayanan et al., 2017; Bergmann et al., 2020). In our DDAD, reconstruction networks are regarded as regressors that regress the gray value at each pixel. Therefore, based on the theory of Deep Ensemble (Lakshminarayanan et al., 2017), the reconstructions' standard deviation can be used to estimate the samples' uncertainty. Specifically, as networks in NDM are trained on only normal images, they will express high difference on their OOD samples, i.e., abnormal regions. Consequently, we propose to use this *intra-discrepancy* inside NDM as an AS:

$$\mathcal{A}_{intra}^p = \sqrt{\frac{1}{K} \sum_{i=1}^K (\hat{\mu}_A^p - \hat{x}_{Ai}^p)^2}, \quad (3)$$

where p is the index of pixels, $\hat{\mu}_A = \frac{1}{K} \sum_{i=1}^K \hat{x}_{Ai}$ is the average map of reconstructions from NDM. Besides, as UDM captures some anomalous features from unlabeled images that NDM never sees, high discrepancy between their outputs will also derive in these abnormal regions. Subsequently, we propose to use the *inter-discrepancy* between the two modules as another AS:

$$\mathcal{A}_{inter}^p = |\hat{\mu}_A^p - \hat{\mu}_B^p|, \quad (4)$$

where $\hat{\mu}_B = \frac{1}{K} \sum_{i=1}^K \hat{x}_{Bi}$ is the average map of reconstructions from UDM. As shown in Fig. 2, our discrepancy maps can indicate potential abnormal regions based on the pixel-wise anomaly scores. The image-level AS is obtained by averaging the pixel-level scores in each image.

Compared with \mathcal{A}_{rec} , our anomaly scores consider the discrepancy between different distributions, leading to stronger discriminative capability. Intuitively, higher AR in unlabeled dataset will lead to greater difference between the distributions of two modules on abnormal regions, deriving more competitive \mathcal{A}_{inter} . Experiments in Section 4.4 validate this hypothesis. In addition, the proposed method can achieve a consistent improvement compared with the reconstruction baseline even if AR is 0, while a low AR can lead to significant boost.

Besides, our discrepancies are all computed among reconstructions, rather than between the input and reconstruction as \mathcal{A}_{rec} does. This can reduce the false positive detection caused by reconstruction ambiguity of AE around high frequency regions (Baur et al., 2021; Mao et al., 2020).

3.4. Uncertainty-refined Anomaly Scores

Due to the reconstruction ambiguity of AE, high reconstruction errors often appear at high frequency regions, e.g., around normal region boundaries, leading to false positive detection. To address this problem, AE-U (Mao et al., 2020) proposed to refine the \mathcal{A}_{rec} using estimated pixel-wise uncertainty. It generates the reconstruction \hat{x}_i and corresponding uncertainty $\sigma^2(x_i)$ for each input x_i , trained by:

$$\mathcal{L} = \frac{1}{NP} \sum_{i=1}^N \sum_{p=1}^P \left\{ \frac{(x_i^p - \hat{x}_i^p)^2}{\sigma_p^2(x_i)} + \log \sigma_p^2(x_i) \right\}. \quad (5)$$

Training on normal images, the numerator of the first term is an *MSE* loss to minimize the reconstruction error, while the

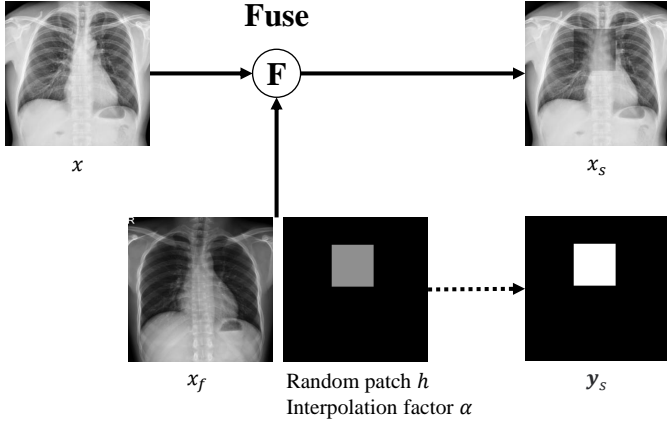


Fig. 4. Illustration of the synthesis of abnormal images. x and x_f denote two different normal images. x_s denotes the synthetic abnormal image and y_s is the corresponding binary pseudo label.

$\sigma_p^2(x_i)$ at the denominator will be learned automatically to be large at pixels with high reconstruction errors to minimize the first term. Besides, the second term drives the predicted uncertainty to be small at other regions. The two loss terms together ensures that the predicted uncertainty will be larger at only normal regions with high reconstruction errors, thus it can be used to refine the anomaly score at pixel-level.

In this work, we design a strategy similar to AE-U while adapting to DDAD well. We use AE-U as the backbone of DDAD, and utilize the uncertainty predicted by our NDM, which is trained on only normal dataset, to refine our intra- and inter-discrepancy at the p -th pixel as:

$$\mathcal{A}_{intra}^p = \frac{\sqrt{\frac{1}{K} \sum_{i=1}^K (\hat{\mu}_A^p - \hat{x}_{Ai}^p)^2}}{\sigma_p}, \quad (6)$$

$$\mathcal{A}_{inter}^p = \frac{|\hat{\mu}_A^p - \hat{\mu}_B^p|}{\sigma_p}, \quad (7)$$

where σ_p is the average uncertainty predicted by AE-U's in NDM.

3.5. Self-supervised Learning-based Anomaly Score Refinement Net

As shown in Fig. 2, the proposed \mathcal{A}_{intra} and \mathcal{A}_{inter} can express high value on abnormal regions, but there are still some noises on normal regions, resulting in false positive detection. To mitigate this problem, we further design an ASR-Net, denoted as $F(\cdot)$, to predict the accurate AS map according to original score maps. Specifically, the network can be formulated as:

$$\mathcal{R}_{dual} = F([\mathcal{A}_{intra}, \mathcal{A}_{inter}]), \quad (8)$$

where the network $F(\cdot)$ refines and fuses the original dual-distribution discrepancies, \mathcal{A}_{intra} and \mathcal{A}_{inter} , to derive the final accurate AS map \mathcal{R}_{dual} .

In order to obtain an effective $F(\cdot)$, we design a self-supervised task, where pseudo abnormal images with corresponding pixel-level binary labels are synthesized to train the

$F(\cdot)$. Specifically, we employee a simple approach for the synthesis of abnormal images reference to FPI (Tan et al., 2020). As shown in Fig. 4, for each normal image x , we assign a random patch h and fuse x with another normal image x_f in the region h with the interpolation α , deriving synthetic abnormal image x_s . The operation is formulated as:

$$x_s^p = (1 - \alpha)x^p + \alpha x_f^p, \forall p \in h, \quad (9)$$

where p is the index of pixels and the interpolation $\alpha \sim U(0, 1)$. The random patch h is restricted by:

$$h_c \sim U(0.1d, 0.9d), h_s \sim U(0.1d, 0.4d), \quad (10)$$

where d is the image width, h_c is the patch center coordinate and h_s is the patch size.

After obtaining the synthetic abnormal image x_s , we feed it forward our well-trained NDM and UDM (i.e., the Stage 1 in Fig. 2), and compute its \mathcal{A}_{intra} and \mathcal{A}_{inter} . With the supervision of corresponding pseudo label y_s , $F(\cdot)$ is then trained by the Focal Loss (Lin et al., 2017) as:

$$\mathcal{L}_R = \text{FL}(F([\mathcal{A}_{intra}, \mathcal{A}_{inter}]), y_s), \quad (11)$$

where the $\text{FL}(\cdot)$ is the Focal Loss function. For each pixel with prediction probability p_t for the ground truth class, the focal loss is computed as:

$$\mathcal{L}_{focal}(p_t) = -(1 - p_t)^\gamma \log(p_t), \quad (12)$$

where γ is the tunable focusing parameter.

Through this way, the ASR-Net $F(\cdot)$ learns to map the original AS to the final accurate abnormal regions as shown in the Stage 2 of Fig. 2, improving the robustness significantly. Different from previous self-supervised anomaly detection methods, ASR-Net learns the aforementioned mapping function, rather than learns to detect the synthetic abnormal patterns, achieving better generalization and less sensitivity to the quality of synthetic images.

In addition, in case that the unlabeled images are not acquired, we also explore the performance of using only \mathcal{A}_{intra} under the same setting as OCC problem. The score map refined by $F(\cdot)$ according to only \mathcal{A}_{intra} is denoted as \mathcal{R}_{intra} :

$$\mathcal{R}_{intra} = F(\mathcal{A}_{intra}). \quad (13)$$

4. Experiments

4.1. Datasets

We conduct extensive experiments on three CXR datasets, one brain MRI dataset, and one retinal fundus image dataset: 1) RSNA Pneumonia Detection Challenge dataset¹, 2) VinBigData Chest X-ray Abnormalities Detection dataset (VinDr-CXR)² (Nguyen et al., 2022), 3) Chest X-ray Anomaly Detection (CXAD) dataset³, and 5)

¹<https://www.kaggle.com/c/rsna-pneumonia-detection-challenge>

²<https://www.kaggle.com/c/vinbigdata-chest-xray-abnormalities-detection>

³<https://www.kaggle.com/datasets/masoudnickparvar/brain-tumor-mri-dataset>

Table 1. Summary of datasets repartition. Note that D_u is built using data selected from the parentheses without the use of their annotations.

Dataset	Repartition		
	Normal Dataset D_n	Unlabeled Dataset D_u	Testing Dataset D_t
RSNA ¹	3851	4000 (4000 normal + 5012 abnormal images)	1000 normal + 1000 abnormal images
VinDr-CXR ² (Nguyen et al., 2022)	4000	4000 (5606 normal + 3394 abnormal images)	1000 normal + 1000 abnormal images
CXAD	2000	2000 (800 normal + 1200 abnormal images)	499 normal + 501 abnormal images
Brain Tumor ³	1000	1000 (400 normal + 2666 abnormal images)	600 normal + 600 abnormal images
LAG (Li et al., 2019)	1500	1500 (832 normal + 900 abnormal images)	811 normal + 811 abnormal images

Large-scale attention based glaucoma (LAG) dataset (Li et al., 2019).

RSNA dataset: The dataset contains 8851 normal and 6012 lung opacity CXRs. In experiments, we use 3851 normal images as the normal dataset D_n , 4000 images with different ARs as the unlabeled dataset D_u , and 1000 normal and 1000 lung opacity images as the test dataset D_t .

VinDr-CXR dataset: The dataset contains 10606 normal and 4394 abnormal CXRs that include 14 categories of anomalies in total. In experiments, we use 4000 normal images as D_n , 4000 images as D_u , and 1000 normal and 1000 abnormal images as D_t .

CXAD dataset: The dataset is collected by us for this study, and contains 3299 normal and 1701 abnormal CXRs that include 18 categories of anomalies in total. In experiments, we use 2000 normal images as D_n , 2000 images as D_u , and 499 normal and 501 abnormal images as D_t .

Brain Tumor dataset: The dataset contains 2000 MRI slices with no tumor, 1621 with glioma, and 1645 with meningioma. Both glioma and meningioma are regarded as anomalies. In experiments, we use 1000 normal images (i.e., with no tumor) as D_n , 1000 images as D_u , and 600 normal and 600 abnormal images (containing 300 with glioma and 300 with meningioma) as D_t .

LAG dataset: The dataset contains 3143 normal retinal fundus images and 1711 abnormal retinal fundus images with glaucoma. In experiments, we use 1500 normal images as D_n , 1500 images as D_u , and 811 normal and 811 abnormal images as D_t .

As a summary, we show the details of aforementioned datasets repartition in Table 1. For the OCC setting, only D_n is used during training. For our proposed training mode, both D_n and D_u are utilized. Except for our private CXAD, the other 4 benchmarks we reorganized and corresponding repartition file will be released for reproducibility. As there are rare public available benchmarks for anomaly detection in medical images, our released benchmarks will significantly contribute to a fair comparison of different researches.

4.2. Implementation Details

The AE in our experiments contains an encoder and a decoder. The encoder contains 4 convolutional layers with kernel size 4 and stride 2, whose channel sizes are 16-32-64-64. The decoder contains 4 deconvolutional layers with the same kernel size and stride as the encoder, and the channel sizes are 64-32-16-1. The encoder and decoder are connected by 3 fully connected layers. All layers except the output layer are followed by batch normalization (BN) and ReLU. For fair comparison, MemAE (Gong et al., 2019) and AE-U (Mao et al., 2020) in

our experiments are modified based on this AE. All the input images are resized to 64×64 . K is set to 3. All the reconstruction models are trained for 250 epochs using the Adam optimizer with a learning rate of $5e-4$.

The proposed ASR-Net consists of three cascade convolutional layers, connected by BN and ReLU. It is trained for 100 epochs with a learning rate of $1e-4$ and a weight decay of $1e-4$ to ensure convergence.

All experiments were implemented using PyTorch and conducted on a single NVIDIA TITAN Xp GPU. The performance is assessed with area under the ROC curve (AUC) and the average precision (AP).

4.3. Comparison with State-of-the-art Methods

In Table 2, we compare our proposed method with several state-of-the-art (SOTA) methods, including MemAE (Gong et al., 2019), Ganomaly (Akçay et al., 2018), CutPaste (Li et al., 2021), DRAEM (Zavrtanik et al., 2021), f-AnoGAN (Schlegl et al., 2019), IGD (Chen et al., 2022) and AE-U (Mao et al., 2020). Note that CutPaste (Li et al., 2021) has not released the official code, thus we use a public implementation from <https://github.com/Runinho/pytorch-cutpaste>. All other methods used in the experiments are implemented using their official codes.

Firstly, we compare our DDAD- \mathcal{R}_{intra} with others under the same OCC setting for fairness, i.e., only normal dataset D_n is used during training without the use of unlabeled images. Under the OCC setting, the best two results are marked in **bold** and underline in Table 2. The results show that our DDAD built on AE-U using \mathcal{R}_{intra} as the AS achieves SOTA results on almost all the 5 benchmarks containing 3 different medical image modalities (CXR, brain MRI and retinal fundus image), demonstrating the effectiveness and generality of our proposed method. Note that CutPaste (Li et al., 2021) and DRAEM (Zavrtanik et al., 2021) are SOTA self-supervised based methods on industrial anomaly detection (Bergmann et al., 2019), but they fail in several medical datasets due to the reliance on the similarity between synthetic abnormal patterns and the real anomalies.

Secondly, we evaluate our proposed method in the situation that unlabeled image dataset D_u is utilized, i.e., use \mathcal{R}_{dual} as the AS. Reference to ARs of several public medical image datasets (e.g., 71% in RSNA, 46% in ChestX-ray8 (Wang et al., 2017) and 62% in Brain Tumor MRI), we generally assume an AR of 60% for D_u in the experiments. Under this setting, the best results are marked in **underlined bold** in Table 2. While our DDAD (AE-U) using \mathcal{R}_{intra} has achieved SOTA results, our

Table 2. Comparison with SOTA methods. For methods that don't use unlabeled images, the best two results are marked in bold and underline. For methods that use unlabeled images, the best results are marked in underline bold.

Unlabeled images	Method	AS	RSNA		VinDr-CXR		CXAD		Brain MRI		LAG	
			AUC	AP	AUC	AP	AUC	AP	AUC	AP	AUC	AP
✗	AE		66.9	66.1	55.9	60.3	55.6	59.6	79.7	71.9	79.3	76.1
	MemAE (Gong et al., 2019)		68.0	67.1	55.8	59.8	56.0	60.0	77.4	70.0	78.5	74.9
	Ganomaly (Akçay et al., 2018)		71.4	69.1	59.6	60.3	62.5	63.0	75.1	69.7	77.7	75.7
	CutPaste (Li et al., 2021)		79.4	74.4	70.2	69.8	53.6	57.3	92.0	89.4	69.1	64.6
	DRAEM (Zavrtanik et al., 2021)		62.3	61.6	63.0	68.3	54.3	55.6	72.1	64.6	47.2	49.0
	f-AnoGAN (Schlegl et al., 2019)		79.8	75.6	76.3	74.8	61.9	<u>67.3</u>	82.5	74.3	<u>84.2</u>	77.5
	IGD (Chen et al., 2022)		81.2	78.0	59.2	58.7	55.2	57.6	94.3	<u>90.6</u>	80.7	75.3
	AE-U (Mao et al., 2020)		86.7	84.7	73.8	72.8	<u>66.4</u>	66.9	94.0	89.0	81.3	<u>78.9</u>
	Ours (AE)	\mathcal{R}_{intra}	86.3	85.5	<u>77.2</u>	74.2	63.8	65.4	85.0	77.6	79.5	74.5
	Ours (MemAE)		<u>87.2</u>	<u>86.1</u>	73.9	72.1	62.4	64.5	82.9	78.6	80.1	77.6
	Ours (AE-U)		88.3	87.6	78.2	<u>74.6</u>	69.4	69.3	<u>94.2</u>	91.9	86.0	84.0
✓	Ours (AE)	\mathcal{R}_{dual}	89.3	89.5	77.4	77.7	65.0	67.2	93.0	87.1	89.0	86.9
	Ours (MemAE)		88.5	87.8	75.3	74.1	63.5	64.3	91.4	84.8	88.7	86.5
	Ours (AE-U)		91.3	91.6	85.9	84.3	71.0	72.7	97.2	95.2	93.1	92.3

\mathcal{R}_{dual} further improves the performance with the help of unlabeled images, outperforming previous methods by a larger margin. These results indicate that our proposed method is able to capture useful information from unlabeled images for anomaly detection successfully.

4.4. Ablation Study

4.4.1. DDAD with different ARs

In clinical practice, the AR of unlabeled dataset D_u is unknown. In order to simulate the various real scenarios, we evaluate the proposed DDAD on RSNA dataset with AR of D_u varying from 0 to 100%. We use the reconstruction method as the baseline for comparison. For fair comparison, all these methods use AE as the backbone. The results of proposed DDAD method using \mathcal{R}_{dual} , \mathcal{R}_{intra} , \mathcal{A}_{inter} and \mathcal{A}_{intra} , and the results of reconstruction baseline are shown in Fig. 5, which demonstrate the effectiveness of our proposed anomaly scores and ASR-Net clearly.

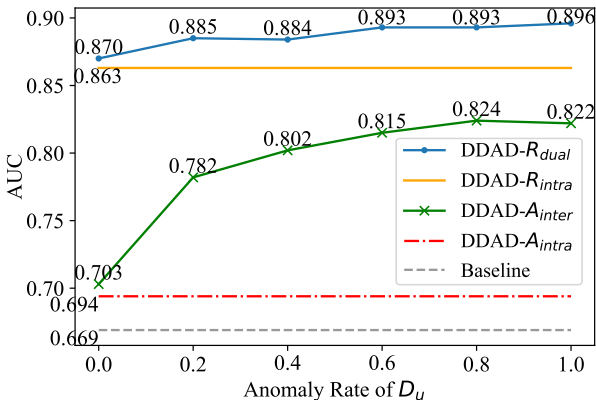


Fig. 5. Performance of DDAD and the reconstruction baseline on RSNA dataset with varying AR of D_u using AE as the backbone.

Firstly, DDAD using the original \mathcal{A}_{intra} and \mathcal{A}_{inter} achieves consistent and significant improvement compared with the reconstruction baseline, suggesting that the proposed two anomaly scores are more discriminative than the previous reconstruction error. Moreover, our \mathcal{A}_{inter} is better than \mathcal{A}_{intra} , while it performs better with the increasing AR of D_u , consistent with our hypothesis in Section 3.3 that higher AR of D_u will result in more competitive \mathcal{A}_{inter} . Because \mathcal{A}_{intra} is computed inside NDM, it's irrelevant to AR. It's worth noting that even in the extreme situation (i.e., AR is 0), our DDAD- \mathcal{A}_{inter} can still achieve better performance than baseline. That's to say, we can apply the DDAD in any situations and get improvement consistently regardless of AR. Intuitively, when AR is 0, dataset $D_n \cup D_u$ only contains normal images, thus UDM degenerates to the same as NDM. However, in this situation UDM is trained on a larger normal dataset than baseline, which leads to more robust models and supports the consistent improvement. Meanwhile, even if AR is low (e.g., 20%), the DDAD can achieve a significant improvement (7.9% AUC higher than when AR is 0). That means the proposed DDAD can improve the performance considerably in clinical practice as there are always some abnormal cases.

Secondly, refined by the proposed ASR-Net, our \mathcal{R}_{dual} and \mathcal{R}_{intra} have a further significant gain compared with the original \mathcal{A}_{inter} and \mathcal{A}_{intra} . Specifically, when using only normal images, our ASR-Net $F(\cdot)$ refines \mathcal{A}_{intra} and derives \mathcal{R}_{intra} , which improves the AUC of \mathcal{A}_{intra} by a large margin of 16.9% (from 69.4% to 86.3%). Incorporating the unlabeled images, we can derive \mathcal{A}_{inter} as a complement of \mathcal{A}_{intra} . The two anomaly scores are refined and fused by $F(\cdot)$, deriving \mathcal{R}_{dual} , which achieves an outstanding AUC of 87.0%–89.6% with the AR of D_u varying from 0 to 100%, outperforming all aforementioned methods. More importantly, while our \mathcal{R}_{dual} utilizes unlabeled images and achieves advanced performance, it's insensitive to the AR of D_u . Even if AR is 0, it can achieve an outstanding AUC of 87.0%, which outperforms \mathcal{A}_{inter} in any situations. Therefore, with the help of ASR-Net, the DDAD is more robust

Table 3. Performance of different methods using three backbones on five datasets. The best two results for each backbone are marked in underlined bold and **bold.**

Method	AS	AUC														
		RSNA			VinDr-CXR			CXAD			Brain Tumor			LAG		
		AE	MemAE	AE-U	AE	MemAE	AE-U	AE	MemAE	AE-U	AE	MemAE	AE-U	AE	MemAE	AE-U
Rec.	\mathcal{A}_{rec}	66.9	68.0	86.7	55.9	55.8	73.8	55.6	56.0	66.4	79.7	77.4	94.0	79.3	78.5	81.3
Rec. (ensemble)		66.9	67.0	86.6	55.5	55.3	73.1	55.0	55.2	65.9	81.3	79.2	93.3	78.8	79.2	82.1
DDAD	\mathcal{A}_{intra}	69.4	72.9	87.3	60.1	59.5	74.3	59.8	59.4	69.2	55.9	52.6	84.5	72.1	71.3	75.3
	\mathcal{A}_{inter}	81.5	78.8	91.0	71.0	69.0	85.9	62.1	59.9	71.4	84.4	83.2	97.1	87.2	88.5	80.6
	\mathcal{R}_{intra}	86.3	87.2	88.3	77.2	73.9	78.2	63.8	62.4	69.4	85.0	82.9	94.2	79.5	80.1	86.0
	\mathcal{R}_{dual}	89.3	88.5	91.3	77.4	75.3	85.9	65.0	64.5	71.0	93.0	91.4	97.2	89.0	88.7	93.1

and it can handle various complex situations in clinical practice well.

4.4.2. DDAD with different backbones

Our proposed DDAD method can use any AEs' variants as backbones. In order to further prove the superiority, DDAD built on different backbones are compared with corresponding reconstruction baselines (Rec.) in Table 3. The best two results for each backbone are marked in underlined bold and **bold**. Consistent with Section 4.3, we also assume an AR of 60% for D_u in experiments. The results show that DDAD based on AE, MemAE (Gong et al., 2019) and AE-U (Mao et al., 2020) can all outperform corresponding baselines on the 5 datasets by a large margin.

Specifically, all of our original \mathcal{A}_{intra} , \mathcal{A}_{inter} , and the refined \mathcal{R}_{intra} , \mathcal{R}_{dual} perform competitively in three CXR datasets (i.e., RSNA, VinDr-CXR and CXAD datasets). In terms of AUC, DDAD- \mathcal{A}_{intra} improves baselines of AE, MemAE and AE-U by 2.5%, 4.9% and 0.6% on RSNA dataset, by 4.2%, 3.7% and 0.5% on VinDr-CXR dataset, by 4.2%, 3.4% and 2.8% on CXAD dataset, respectively. DDAD- \mathcal{A}_{inter} improves baselines of AE, MemAE and AE-U by 14.6%, 10.8% and 4.3% on RSNA dataset, by 15.1%, 13.2% and 12.1% on VinDr-CXR dataset, by 6.5%, 3.9% and 5.0% on CXAD dataset, respectively. With the help of our ASR-Net, DDAD- \mathcal{R}_{intra} improves baselines of AE, MemAE and AE-U by 19.4%, 19.2% and 1.6% on RSNA dataset, by 21.3%, 18.1% and 4.4% on VinDr-CXR dataset, by 8.2%, 6.4% and 3.0% on CXAD dataset, respectively. DDAD- \mathcal{R}_{dual} improves baselines of AE, MemAE and AE-U by 22.4%, 20.5% and 4.6% on RSNA dataset, by 21.5%, 19.5% and 12.1% on VinDr-CXR dataset, by 9.4%, 7.5% and 4.6% on CXAD dataset, respectively.

As for the Brain Tumor and LAG dataset, the proposed original \mathcal{A}_{intra} performs worse than the corresponding reconstruction baseline. However, with the aid of our ASR-Net, the \mathcal{R}_{intra}

can significantly improve the performance of \mathcal{A}_{intra} and outperform corresponding baseline by a large margin. The reason could be that although the original \mathcal{A}_{intra} contains noises and works unsatisfactorily, it does encode useful information for anomaly detection, which is extracted by our ASR-Net successfully, deriving the \mathcal{R}_{intra} . Finally, consistent with the results on three CXR datasets, on the Brain Tumor and LAG datasets our refined \mathcal{R}_{intra} and \mathcal{R}_{dual} outperform the original \mathcal{A}_{intra} and \mathcal{A}_{inter} , respectively, while showing superiority to reconstruction baselines.

We also test the ensemble of K reconstruction models using \mathcal{A}_{rec} , i.e., Rec. (ensemble) in Table 3, demonstrating that simple ensemble has no significant improvement. The reason why some ensembles result in slightly worse performance could be that the average reconstruction of ensemble networks may generalize better than the single network on some abnormal regions, causing reconstruction errors in these regions indistinguishable from those of normal regions.

4.5. Qualitative Analysis

To further illustrate the superiority of the proposed method explicitly, we conduct qualitative analysis on the RSNA dataset in this section using AS histograms and score maps.

4.5.1. AS histograms

To show the discriminative capability of different methods, we visualize the histograms of their AS for normal and abnormal images in Fig. 6 using AE as the backbone. The overlaps of normal and abnormal histograms indicate samples with the same anomaly score but different categories, thus indistinguishable. The χ^2 -distance shown in figures measures the difference between the histograms of normal and abnormal images. Therefore, higher difference between the anomaly scores of normal and abnormal images will result in less overlaps and larger χ^2 -distance, indicating stronger discriminative capability. Based

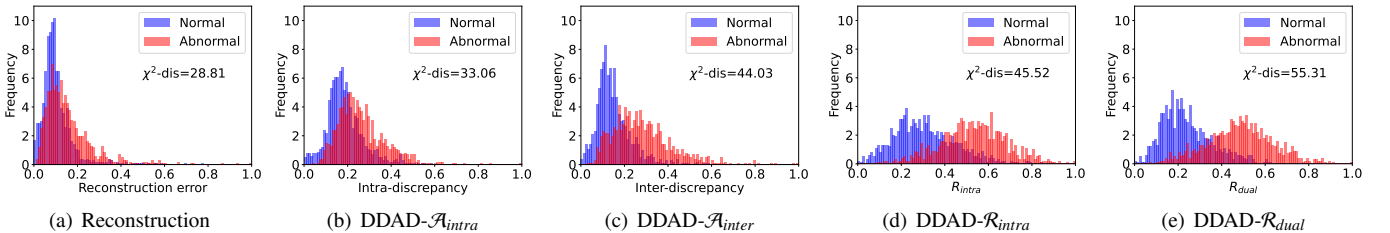


Fig. 6. Histograms of anomaly score for normal (blue) and abnormal (red) images in the test set of RSNA. The backbone is AE. Scores are normalized to [0,1]. The χ^2 -distance measures the difference between the histograms of normal and abnormal images.

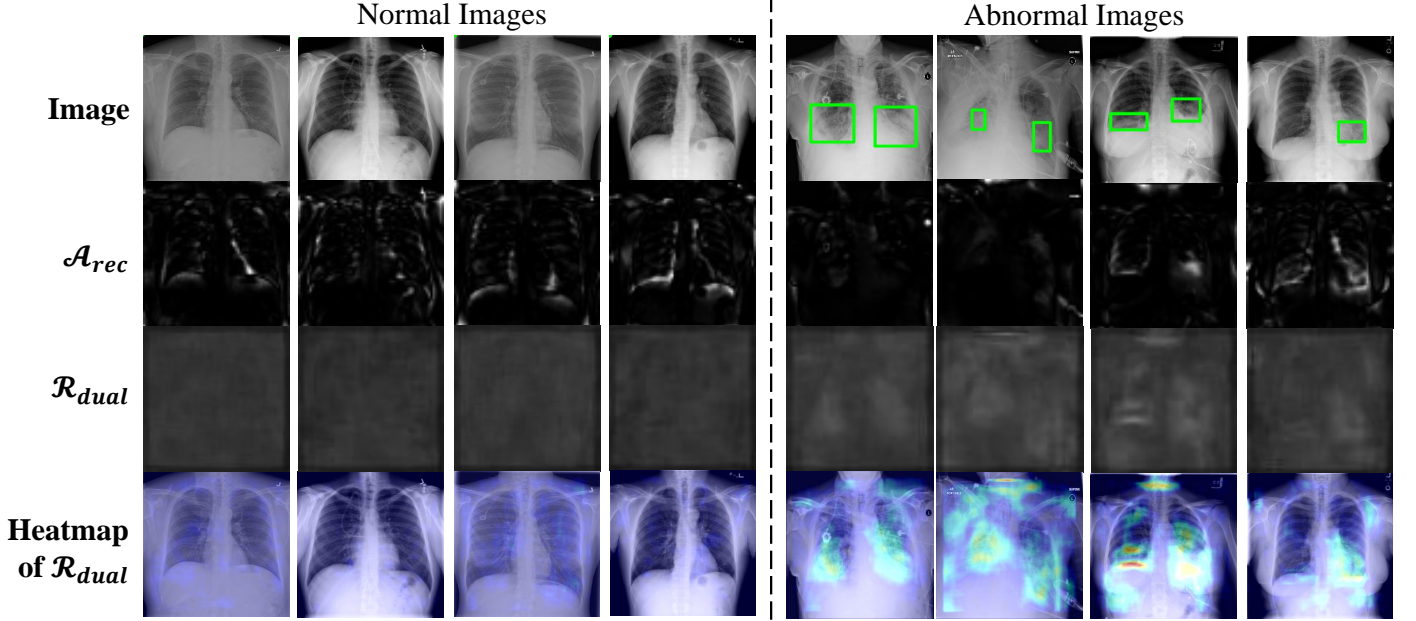


Fig. 7. Visualization of score maps and heat maps on RSNA dataset. The green bounding boxes indicate abnormal regions.

on these analysis and observation, we can draw the conclusion that the proposed DDAD is better than previous reconstruction methods and our ASR-Net is effective. Specifically, the performance of different methods (anomaly scores) can be ranked from better to worse as: \mathcal{R}_{dual} and $\mathcal{R}_{intra} > \mathcal{A}_{inter}$ and $\mathcal{A}_{intra} > \mathcal{A}_{rec}$, which is consistent with our experimental results.

4.5.2. Score maps

We visualize score maps of reconstruction method and our proposed DDAD, using AE as the backbone for fair comparison, on the RSNA dataset. As shown in Fig. 7, previous reconstruction method (\mathcal{A}_{rec}) always has false positive detection on normal regions, especially around boundary regions with high frequency. Besides, it can't identify some subtle lesions well, resulting in false negative detection. In contrast, our DDAD- \mathcal{R}_{dual} expresses high response on even subtle abnormal regions and low response on normal regions, which can be utilized as a localization result for reference to radiologists.

5. Discussion

This study present a novel anomaly detection method using designed dual-distribution discrepancy with self-supervised refinement. To our knowledge, it's the first attempt to utilize unlabeled images as a complement of normal images to realize a better anomaly detection. The proposed approach outperforms SOTA methods on five medical benchmarks, which validates the effectiveness of our intra- and inter-discrepancy and the ASR-Net. Based on the observations from Section 4, there are some noteworthy advantages and limitations to discuss, which could indicate the future direction.

The results show that our ASR-Net based on self-supervised learning improve the performance a lot on the five benchmarks. However, other SOTA self-supervised methods (e.g., CutPaste

(Li et al., 2021) and DRAEM (Zavrtanik et al., 2021)) fail in several medical benchmarks, although they can achieve competitive performance on the industrial defect detection benchmark (Bergmann et al., 2019). This phenomenon is highly related to what these networks learn through self-supervised learning. For CutPaste (Li et al., 2021) and DRAEM (Zavrtanik et al., 2021), their models are directly trained to detect synthetic abnormal patterns, which are similar to industrial defects but dissimilar to medical anomalies, thus they can't distinguish abnormal medical images from healthy ones. In contrast, our ASR-Net learns the mapping function from the original AS to the final accurate abnormal regions, which are unrelated to the abnormal patterns, thus generalize well to anomalies of different modalities, including CXR, MRI and retinal fundus image. Therefore, compared with previous self-supervised anomaly detection methods that focus on synthesis of anomalies, designing self-supervised tasks that are insensitive to the abnormal patterns is more general, promising and competitive in complex real scenarios.

Currently, limitations of our ASR-Net also exist. In the experiments, the ASR-Net has only a small improvement when the original dual-distribution discrepancy AS refined by the uncertainty from AE-U already achieves a high performance (i.e., DDAD (AE-U) in Table 3). The reason could be that our refinement strategy is conducted on the discrepancy maps of ensembles of reconstruction networks, causing that the upper bound of performance is limited by the distribution-modeling capability of these reconstruction networks. Therefore, some subtle abnormal regions that are reconstructed consistently by different networks in the ensemble are unable to be recognized regardless of the subsequent refinement. In the future work, we intend to explore a single network that models the distribution of training data explicitly to improve the distribution-modeling capability and achieve a higher upper bound of performance.

Besides, although our approach takes use of unlabeled images successfully, a number of normal images are still required for training, which can also be time-consuming to collect in practice. Recently, [Zaheer et al. \(2022\)](#) proposed the generative cooperative learning (GCL) approach for anomaly detection, which is trained using only unlabeled images where normal samples are the majority. They designed a co-training strategy of an auto-encoder and a classifier to generate pseudo labels for unlabeled images, revealing the feasibility of anomaly detection using only unlabeled training data. Inspired by this, we intend to explore a more effective pseudo label generation approach with reference to methods of learning with noisy labels ([Wei et al., 2020](#); [Jiang et al., 2018](#); [Han et al., 2018](#)), to develop a powerful anomaly detection framework without the requirement of any training annotations.

Considering these current limitations, we summarize several promising future directions of anomaly detection: 1) unsupervised anomaly detection ([Zaheer et al., 2022](#)) (using only unlabeled images for training to detect anomalies), 2) open-set supervised anomaly detection ([Ding et al., 2022](#)) (using a few labeled abnormal images and normal images for training to detect both seen anomalies and unseen anomalies), and 3) few-shot anomaly detection ([Huang et al., 2022](#)) (using only a limited number of normal images for training to detect anomalies). Actually, the first step for handling the unsupervised anomaly detection is to generate reasonable pseudo labels for unlabeled training images. Obtained these pseudo normal or abnormal labels for training data, the task 1) can be converted to 2) and 3).

To explore these three new directions, there are several challenges to be studied. Firstly, abnormal medical images only have subtle difference to normal ones, which could be difficult to be assigned with accurate pseudo labels by current methods for learning with noisy labels ([Wei et al., 2020](#)), where predictions are made by vanilla classification networks according to the whole image. Another challenge is that classes of anomalies are inexhaustible. Even if some abnormal images are labeled accurately, incorporating them in training can render models ineffective in generalizing to unseen anomaly classes. In summary, fine-grained models that is able to recognize subtle lesions and a new training paradigm for utilizing limited labeled images are in high demand for anomaly detection.

6. Conclusion

In this paper, we propose the Dual-distribution Discrepancy for Anomaly Detection (DDAD), which fully utilizes both known normal and unlabeled images. Two new anomaly scores, intra- and inter-discrepancy, are designed based on DDAD for identifying anomalies. In addition, an Anomaly Score Refinement Net (ASR-Net) trained via self-supervised learning is designed to refine and fuse the two anomaly scores, obtaining the final accurate prediction. To facilitate the fair and comprehensive comparison of different methods, we collect and organize five medical datasets including three modalities and release them as benchmarks for medical anomaly detection. Experiments on the five benchmarks demonstrate that the proposed

DDAD with the ASR-Net is effective and general, achieving state-of-the-art performance on a wide variety of medical images. As the first method that utilizes readily available unlabeled images to improve performance of anomaly detection, we hope this work will inspire researchers to explore anomaly detection in a more effective way. Besides, we also hope our released benchmarks for medical anomaly detection will encourage more researchers in this field to compare their methods fairly and ensure the reproducibility.

Acknowledgments

This work was supported in part by Hong Kong Innovation and Technology Fund (No. ITS/028/21FP), National Natural Science Foundation of China (61872417, 62061160490, 62176098, 61703049) and Natural Science Foundation of Hubei Province of China (2019CFA022).

References

- Akçay, S., Atapour-Abarghouei, A., Breckon, T.P., 2018. Ganomaly: Semi-supervised anomaly detection via adversarial training, in: Asian conference on computer vision, Springer. pp. 622–637.
- Baur, C., Denner, S., Wiestler, B., Navab, N., Albarqouni, S., 2021. Autoencoders for unsupervised anomaly segmentation in brain mr images: a comparative study. *Medical Image Analysis* 69, 101952.
- Baur, C., Wiestler, B., Albarqouni, S., Navab, N., 2018. Deep autoencoding models for unsupervised anomaly segmentation in brain mr images, in: International MICCAI brainlesion workshop, Springer. pp. 161–169.
- Beluch, W.H., Genewein, T., Nürnberger, A., Köhler, J.M., 2018. The power of ensembles for active learning in image classification, in: Proceedings of the IEEE conference on computer vision and pattern recognition, pp. 9368–9377.
- Bergmann, P., Fauser, M., Sattlegger, D., Steger, C., 2019. Mvtec ad—a comprehensive real-world dataset for unsupervised anomaly detection, in: Proceedings of the IEEE/CVF conference on computer vision and pattern recognition, pp. 9592–9600.
- Bergmann, P., Fauser, M., Sattlegger, D., Steger, C., 2020. Uninformed students: Student-teacher anomaly detection with discriminative latent embeddings, in: Proceedings of the IEEE/CVF Conference on Computer Vision and Pattern Recognition, pp. 4183–4192.
- Cai, Y., Chen, H., Yang, X., Zhou, Y., Cheng, K.T., 2022. Dual-distribution discrepancy for anomaly detection in chest x-rays, in: International Conference on Medical Image Computing and Computer-Assisted Intervention, Springer. pp. 584–593.
- Çalli, E., Sogancioglu, E., van Ginneken, B., van Leeuwen, K.G., Murphy, K., 2021. Deep learning for chest x-ray analysis: A survey. *Medical Image Analysis* 72, 102125.
- Chandola, V., Banerjee, A., Kumar, V., 2009. Anomaly detection: A survey. *ACM computing surveys (CSUR)* 41, 1–58.
- Chen, X., Konukoglu, E., 2018. Unsupervised detection of lesions in brain mri using constrained adversarial auto-encoders. *arXiv preprint arXiv:1806.04972*.
- Chen, Y., Tian, Y., Pang, G., Carneiro, G., 2022. Deep one-class classification via interpolated gaussian descriptor, in: Proceedings of the AAAI Conference on Artificial Intelligence, pp. 383–392.
- Cheplygina, V., de Bruijne, M., Pluim, J.P., 2019. Not-so-supervised: a survey of semi-supervised, multi-instance, and transfer learning in medical image analysis. *Medical image analysis* 54, 280–296.
- Ding, C., Pang, G., Shen, C., 2022. Catching both gray and black swans: Open-set supervised anomaly detection, in: Proceedings of the IEEE/CVF Conference on Computer Vision and Pattern Recognition, pp. 7388–7398.
- Doersch, C., Gupta, A., Efros, A.A., 2015. Unsupervised visual representation learning by context prediction, in: Proceedings of the IEEE international conference on computer vision, pp. 1422–1430.
- Golan, I., El-Yaniv, R., 2018. Deep anomaly detection using geometric transformations. *Advances in neural information processing systems* 31.

- Gong, D., Liu, L., Le, V., Saha, B., Mansour, M.R., Venkatesh, S., Hengel, A.v.d., 2019. Memorizing normality to detect anomaly: Memory-augmented deep autoencoder for unsupervised anomaly detection, in: *Proceedings of the IEEE/CVF International Conference on Computer Vision*, pp. 1705–1714.
- Goodfellow, I., Pouget-Abadie, J., Mirza, M., Xu, B., Warde-Farley, D., Ozair, S., Courville, A., Bengio, Y., 2014. Generative adversarial nets. *Advances in neural information processing systems* 27.
- Han, B., Yao, Q., Yu, X., Niu, G., Xu, M., Hu, W., Tsang, I., Sugiyama, M., 2018. Co-teaching: Robust training of deep neural networks with extremely noisy labels. *Advances in neural information processing systems* 31.
- Huang, C., Guan, H., Jiang, A., Zhang, Y., Spratlin, M., Wang, Y., 2022. Registration based few-shot anomaly detection, in: *European Conference on Computer Vision*.
- Jiang, L., Zhou, Z., Leung, T., Li, L.J., Fei-Fei, L., 2018. Mentornet: Learning data-driven curriculum for very deep neural networks on corrupted labels, in: *International conference on machine learning*, PMLR. pp. 2304–2313.
- Jing, L., Tian, Y., 2020. Self-supervised visual feature learning with deep neural networks: A survey. *IEEE transactions on pattern analysis and machine intelligence* 43, 4037–4058.
- Jun, H., Child, R., Chen, M., Schulman, J., Ramesh, A., Radford, A., Sutskever, I., 2020. Distribution augmentation for generative modeling, in: *International Conference on Machine Learning*, PMLR. pp. 5006–5019.
- Krizhevsky, A., Sutskever, I., Hinton, G.E., 2012. Imagenet classification with deep convolutional neural networks. *Advances in neural information processing systems* 25.
- Lakshminarayanan, B., Pritzel, A., Blundell, C., 2017. Simple and scalable predictive uncertainty estimation using deep ensembles. *Advances in neural information processing systems* 30.
- Li, C.L., Sohn, K., Yoon, J., Pfister, T., 2021. Cutpaste: Self-supervised learning for anomaly detection and localization, in: *Proceedings of the IEEE/CVF Conference on Computer Vision and Pattern Recognition*, pp. 9664–9674.
- Li, L., Xu, M., Wang, X., Jiang, L., Liu, H., 2019. Attention based glaucoma detection: a large-scale database and cnn model, in: *Proceedings of the IEEE/CVF conference on computer vision and pattern recognition*, pp. 10571–10580.
- Li, W., Mahadevan, V., Vasconcelos, N., 2013. Anomaly detection and localization in crowded scenes. *IEEE transactions on pattern analysis and machine intelligence* 36, 18–32.
- Lin, T.Y., Goyal, P., Girshick, R., He, K., Dollár, P., 2017. Focal loss for dense object detection, in: *Proceedings of the IEEE international conference on computer vision*, pp. 2980–2988.
- Luo, L., Chen, H., Zhou, Y., Lin, H., Heng, P.A., 2021. Oxnet: Deep omni-supervised thoracic disease detection from chest x-rays, in: *International Conference on Medical Image Computing and Computer-Assisted Intervention*, Springer. pp. 537–548.
- Luo, L., Yu, L., Chen, H., Liu, Q., Wang, X., Xu, J., Heng, P.A., 2020. Deep mining external imperfect data for chest x-ray disease screening. *IEEE transactions on medical imaging* 39, 3583–3594.
- Mao, Y., Xue, F.F., Wang, R., Zhang, J., Zheng, W.S., Liu, H., 2020. Abnormality detection in chest x-ray images using uncertainty prediction autoencoders, in: *International Conference on Medical Image Computing and Computer-Assisted Intervention*, Springer. pp. 529–538.
- Marimont, S.N., Tarroni, G., 2021. Anomaly detection through latent space restoration using vector quantized variational autoencoders, in: *2021 IEEE 18th International Symposium on Biomedical Imaging (ISBI)*, IEEE. pp. 1764–1767.
- Nguyen, H.Q., Lam, K., Le, L.T., Pham, H.H., Tran, D.Q., Nguyen, D.B., Le, D.D., Pham, C.M., Tong, H.T., Dinh, D.H., et al., 2022. Vindr-cxr: An open dataset of chest x-rays with radiologist’s annotations. *Scientific Data* 9, 1–7.
- Ruff, L., Kauffmann, J.R., Vandermeulen, R.A., Montavon, G., Samek, W., Kloft, M., Dietterich, T.G., Müller, K.R., 2021. A unifying review of deep and shallow anomaly detection. *Proceedings of the IEEE*.
- Ruff, L., Vandermeulen, R., Goernitz, N., Deecke, L., Siddiqui, S.A., Binder, A., Müller, E., Kloft, M., 2018. Deep one-class classification, in: *International conference on machine learning*, PMLR. pp. 4393–4402.
- Schlegl, T., Seeböck, P., Waldstein, S.M., Langs, G., Schmidt-Erfurth, U., 2019. f-anogan: Fast unsupervised anomaly detection with generative adversarial networks. *Medical image analysis* 54, 30–44.
- Schlegl, T., Seeböck, P., Waldstein, S.M., Schmidt-Erfurth, U., Langs, G., 2017. Unsupervised anomaly detection with generative adversarial networks to guide marker discovery, in: *International conference on information processing in medical imaging*, Springer. pp. 146–157.
- Schölkopf, B., Williamson, R.C., Smola, A., Shawe-Taylor, J., Platt, J., 1999. Support vector method for novelty detection. *Advances in neural information processing systems* 12.
- Sohn, K., Li, C.L., Yoon, J., Jin, M., Pfister, T., 2020. Learning and evaluating representations for deep one-class classification. *arXiv preprint arXiv:2011.02578*.
- Sultani, W., Chen, C., Shah, M., 2018. Real-world anomaly detection in surveillance videos, in: *Proceedings of the IEEE conference on computer vision and pattern recognition*, pp. 6479–6488.
- Tan, J., Hou, B., Batten, J., Qiu, H., Kainz, B., 2020. Detecting outliers with foreign patch interpolation. *arXiv preprint arXiv:2011.04197*.
- Tan, J., Hou, B., Day, T., Simpson, J., Rueckert, D., Kainz, B., 2021. Detecting outliers with poisson image interpolation, in: *International Conference on Medical Image Computing and Computer-Assisted Intervention*, Springer. pp. 581–591.
- Tian, Y., Pang, G., Liu, F., Chen, Y., Shin, S.H., Verjans, J.W., Singh, R., Carneiro, G., 2021. Constrained contrastive distribution learning for unsupervised anomaly detection and localisation in medical images, in: *International Conference on Medical Image Computing and Computer-Assisted Intervention*, Springer. pp. 128–140.
- Wang, X., Peng, Y., Lu, L., Lu, Z., Bagheri, M., Summers, R.M., 2017. Chestx-ray8: Hospital-scale chest x-ray database and benchmarks on weakly-supervised classification and localization of common thorax diseases, in: *Proceedings of the IEEE conference on computer vision and pattern recognition*, pp. 2097–2106.
- Wei, H., Feng, L., Chen, X., An, B., 2020. Combating noisy labels by agreement: A joint training method with co-regularization, in: *Proceedings of the IEEE/CVF Conference on Computer Vision and Pattern Recognition*, pp. 13726–13735.
- Zaheer, M.Z., Lee, J.h., Astrid, M., Lee, S.I., 2020. Old is gold: Redefining the adversarially learned one-class classifier training paradigm, in: *Proceedings of the IEEE/CVF Conference on Computer Vision and Pattern Recognition*, pp. 14183–14193.
- Zaheer, M.Z., Mahmood, A., Khan, M.H., Segu, M., Yu, F., Lee, S.I., 2022. Generative cooperative learning for unsupervised video anomaly detection, in: *Proceedings of the IEEE/CVF Conference on Computer Vision and Pattern Recognition*, pp. 14744–14754.
- Zavrtanik, V., Kristan, M., Skočaj, D., 2021. Draem-a discriminatively trained reconstruction embedding for surface anomaly detection, in: *Proceedings of the IEEE/CVF International Conference on Computer Vision*, pp. 8330–8339.
- Zimmerer, D., Kohl, S.A., Petersen, J., Isensee, F., Maier-Hein, K.H., 2018. Context-encoding variational autoencoder for unsupervised anomaly detection. *arXiv preprint arXiv:1812.05941*.